PREDICTION OF THE BROADBAND NOISE OF A LOW-SPEED AXIAL FAN BY CFD SIMULATIONS

Alain GUEDEL, Mirela ROBITU

CETIAT, 25 avenue des Arts, B.P. 52042, 69100 Villeurbanne, France

SUMMARY

An extensive research programme has been conducted since several years by CETIAT with scientific and industrial partners to predict one of the major broadband noise sources of low-speed axial fans, namely the blade trailing-edge noise. In a first part of the paper, comparisons of measured and predicted fan sound power spectra due to this mechanism are presented and discussed. The second part of the paper is devoted to the prediction of the wall-pressure fluctuation spectra on the blades of the test fan. These spectra are the main input data of the trailing-edge noise model used. The prediction is made with an empirical model using results of RANS simulations of the flow in the blade boundary-layer.

INTRODUCTION

Broadband noise is a major part of the noise radiated by axial fans. For low-speed fans the contribution of the broadband noise to the overall A-weighted sound power level is indeed often much higher than the contribution of the tonal noise at harmonics of the blade passage frequency. The main broadband noise sources of axial-flow fans are [1]:

- interaction of blades with inflow turbulence
- vortex shedding noise
- tip-clearance noise
- rotating stall
- blade trailing-edge noise.

The first mechanism provides a major contribution when the flow at the fan inlet is significant, typically when the turbulence intensity is higher than 2 to 2.5%, which is the case for instance on an axial fan behind a heat exchanger. This source should be almost negligible when the fan operates in a non-disturbed flow field such as at the entrance of a free-inlet axial fan with a well-designed inlet bell and a fan drive either far upstream or far downstream of the impeller.

Vortex shedding noise, associated with von Karman vortices in the blade wake, occurs when the thickness of the blade trailing edge is larger than the boundary layer thickness. A sharp trailing edge is therefore beneficial to suppress this mechanism.

Tip-clearance noise is due to the interaction of the flow in the tip clearance with the blade. The amplitude of this source usually decreases when the clearance is reduced but the actual noise

mechanism is not yet well understood due to the complex flow pattern in the blade tip area. As shown later in the paper it is certainly an important contributor to the noise of the fan under study.

Rotating stall, which occurs at reduced flow rates and is due to aerodynamic flow instabilities, substantially increases the amount of noise at low frequency.

Blade-trailing edge noise occurs when the turbulent boundary layer on the blade suction side is convected past the trailing edge, a part of the turbulent energy being converted into acoustic energy that radiates to the far-field. This source, which most often prevails over the other sources when the inlet turbulence is low, corresponds to the minimum noise level radiated by the fan. The mechanism remains more or less the same if the boundary layer is attached or separated, even if the noise spectrum is quite different depending on the boundary layer characteristics.

The objective of this paper is, in a first part, to present an overview of experimental and prediction results obtained on a propeller fan of 800 mm diameter with two or four blades in order to validate an analytical model of fan blade trailing-edge noise. This model is based on an extension of Amiet's formulation on isolated airfoil, due to Roger and Moreau [2]. This model was experimentally validated first on fixed airfoils in wind tunnels (see for example [3], [4]) then, to a lesser extent, on rotating blades [5] - **[8**]. The prediction uses the frequency spectra and spanwise correlation length scales of the wall-pressure fluctuations near the trailing edge of the blades as input data. These data may be measured with pressure transducers set on the blades, but this method is tricky and expensive. An alternative is to try to deduce the wall-pressure spectra from an empirical model due to Rozenberg et al. [9], in which the input data are obtained from CFD simulations. This is the topic of the second part of the paper.

EXPERIMENTAL VALIDATION OF THE TRAILING-EDGE NOISE MODEL

Theoretical background

Isolated airfoil in wind-tunnel

The trailing-edge noise prediction is made with an extension of Amiet's analytical formulation for an isolated airfoil. This extension proposed by Roger and Moreau [2], [4] accounts for the effects of a finite chord length and far-field radiation away from the mid-span plane. According to[6] the far-field sound pressure spectrum radiated in the mid-span plane by a fixed airfoil in a uniform flow field is:

$$S_{pp}(\vec{x},\omega) = \left(\frac{kc\sin\theta}{2\pi R}\right)^2 \frac{L}{2}\left|L'\left(x_1,\frac{\omega}{U_c},0\right)\right|^2 \Phi_{pp}(\omega) l_y(\omega) \qquad (1)$$

where:

S_{pp}: sound pressure spectrum (dB/Hz)
R: distance between the mid-span trailing edge and the observer (m)
x_1: coordinate of the observer along the airfoil chord
θ: angle between the chordwise and the observer directions ($\theta = 0°$ in the downstream direction)
c, L: airfoil chord length, airfoil span (m)
$|L'|$ aeroacoustic transfer function
Φ_{pp} spectrum of the turbulent wall-pressure fluctuations (dB/Hz)
l_y: spanwise correlation length of the wall-pressure fluctuations (m)
ω: angular frequency (rad/s) and k: acoustic wavenumber (m^{-1})
U_c: convection velocity of the wall-pressure fluctuations (m/s).

Equation (1) applies to a non-compact airfoil with large aspect ratio (L/c > 1). The equation is more complicated for an airfoil of small aspect ratio and when the observer is away from the airfoil mid-

span [2]. Furthermore, Amiet's formulation strictly applies to slightly loaded airfoils with small camber, thickness and angle of attack, but it has been shown that these restrictions could be relaxed.

The statistics of the turbulent wall-pressure fluctuations, namely the frequency spectrum and the spanwise correlation length, are the input data of the model. The aeroacoustic transfer function L' between the turbulent wall-pressure fluctuations and the far-field sound pressure fluctuations is determined analytically on the basis of purely acoustic arguments. Its expression, given in [2], is a function of chord length c, mean flow velocity U_0, convection velocity of the wall-pressure fluctuations near the trailing edge U_c, and frequency f.

Very good agreements have been obtained between predicted and measured far-field sound pressure spectra for a flat plate [6] as well as for single airfoils of various shapes at different angles of attack in anechoic wind tunnels [1].

Rotating blades

For rotating blades at low rotation Mach number, which is the case here, the above model may be applied with the following adjustment. The blade is split into several strips along its span[1] (strip theory assumption) and the airfoil theory is applied to each segment, assuming that the circular motion is locally equivalent to a translational motion. This assumption is reliable if the trailing-edge noise frequencies are much higher than the rotational frequency. Furthermore, the assumption of blades of large aspect ratio used in equation (1) is no more valid since the span of each segment is smaller than the chord. A more general equation [1], valid for any blade aspect ratio and any angle of observation with respect to the airfoil, is thus applied in the noise prediction of rotating blades.

The far-field sound radiation from a given rotating segment is obtained by averaging the sound pressure spectra radiated by the blade segment at several circumferential locations, applying a Doppler factor to account for the relative motion of the source with respect to the observer. The flow velocity is assumed parallel to the chord line according to the weakly loaded airfoil assumption. As stated in [10] the transposition formula is written as:

$$S_{pp}(\vec{x},\omega) = \frac{B}{2\pi}\int_0^{2\pi} \frac{\omega_e(\Psi)}{\omega}\, S_{pp}^{\Psi}(\vec{x},\omega_e)\, d\Psi \qquad (2)$$

where $S_{pp}^{\Psi}(\vec{x},\omega_e)$ is the sound pressure spectrum that is radiated from the current blade segment at angle Ψ ignoring the Doppler frequency shift, and $\frac{\omega_e(\Psi)}{\omega} = 1 + M\sin\Theta\sin\Psi = 1 - M_r$ where (Θ,Ψ) are the radiation angle to the axis and the circumferential angle, respectively. As Amiet's formulation applies to isolated airfoils this approach is valid for low solidity impellers (chord length smaller than blade spacing). Furthermore, in a recent paper [11] the exponent of the Doppler Shift $\omega_e(\Psi)/\omega$ in equation (2) has been assessed to be 2 instead of 1. At low Mach number M, which is the case in this paper, the effect of this correction on the prediction is negligible.

Experimental validation on axial fans

An extensive research program has been made at CETIAT on a 2-blade (Figure 1-a) and a 4-blade (Figure 1-b) axial fan of 800-mm diameter with the motor and its support on the fan inlet side. The fans with identical blades in plastic have the characteristics given in Table 1.

Table 1 characteristics of the fan used for experimental validation

[1] A division of the blade into 6 strips on the span is a good compromise as found in a preliminary study. This number of strips was kept constant in all the predictions.

Tip radius r_0 (mm)	Hub/Tip ratio	Chord length (mm)	Maximum blade thickness (mm)	Blade pitch angle β (°)	Average tip clearance (mm)	Rotation speed (rpm)
400	0.34	135 at the tip	4	adjustable from 15 to 35° (tip angle counted from the rotation plane)	5	600

To obtain the input data of the model two opposite blades are fitted with a set of 6 small flush-mounted microphones at two radial positions r/r_0 = 0.67 and 0.89. These pressure transducers (Knowles Acoustics microphones) have a diameter and a length of 2.5 mm. They are imbedded on the suction side of the blades as shown by the white lines in Figure 1. Four transducers are on the same spanwise line at 10 mm from the trailing edge to obtain the average spectra and correlation length scales of the wall-pressure fluctuations. The two others are 5 mm chordwisely spaced from the formers to deduce the convection speed of the turbulent pressure fluctuations that is used in the aeroacoustic transfer function $|L'|$ in equation (1). More details on the insertion of the pressure transducers in the blades and their calibration are given in [10]. The signals of the transducers are transmitted to the spectrum analyzer via a 14-channel slip ring.

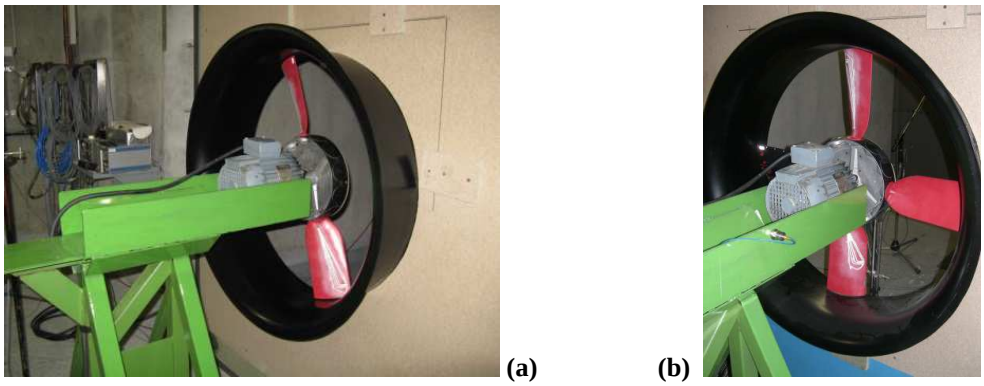

Figure 1 Test fans: (a) 2 blades, (b) 4 blades

The axial location of the impeller in the fan casing has been set to have the blade trailing-edge section in the same plane as the shroud exit section for a blade pitch angle β = 30°.

Each fan is tested in a double reverberant room (Figure 2) according to test category A (non-ducted at inlet and outlet). The fan is mounted on the concrete partition[2] between the two rooms of different sizes, the bigger room being on the inlet side. The auxiliary fan allows adjusting the operating point of the test fan. The flowrate is measured with a multi-nozzle chamber while the fan pressure is obtained according to ISO 5801 with pressure rings in the two reverberant rooms.

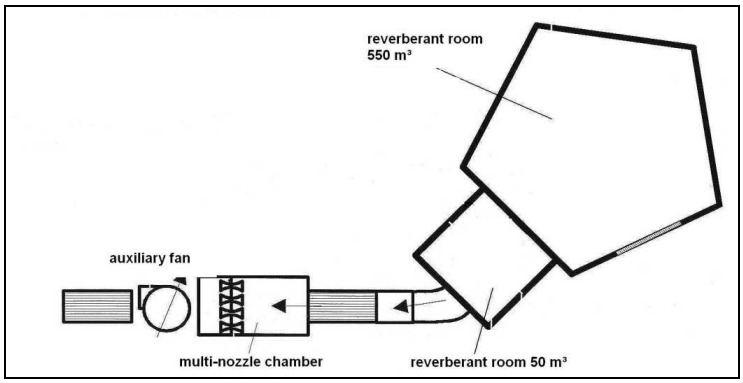

Figure 2 CETIAT test facility layout

The fan sound power levels in one-third octave bands are determined in both rooms following ISO 13347-2. For each frequency band the logarithmic sum of the levels in the two rooms, called "inlet + outlet" level, is thus compared to the prediction.

[2] The fan shroud is actually mounted on a chipboard plate which is fixed to the concrete wall via a gasket

Figure 3 shows the measured sound power spectra of the 2-blade and 4-blade fans for a blade pitch angle of 30° and different operating points identified by their flowrate expressed as a fraction of the maximum flow Qv max (i.e. zero static pressure) of each fan.

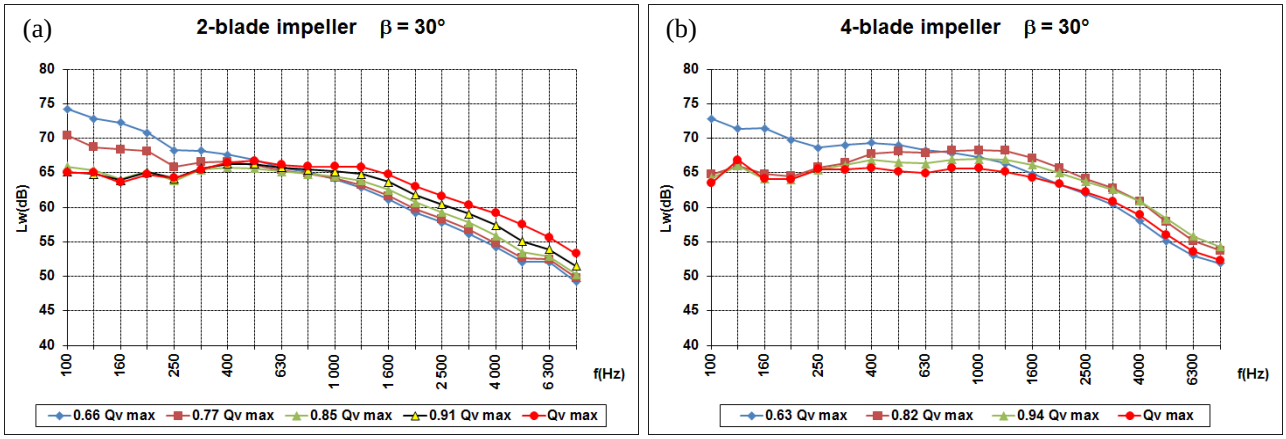

Figure 3 Measured "inlet + outlet" sound power levels for β = 30° (a) 2-blade fan, (b) 4-blade fan

As mentioned above the main input data of the analytical prediction model are the spectra and spanwise correlation scales of the blade pressure fluctuations. For the 4-blade fan with β = 30° and various operating points, Figure 4 shows the measured wall-pressure spectra in one-third octave band and Figure 5 presents the measured spanwise correlation scales of the blade pressure fluctuations as a function of frequency for the two sets of pressure transducers.The reference of the decibel scale of the wall-pressure spectra is set to 2.10^{-5} Pa, like the acoustic pressure, even if those pressure fluctuations are purely aerodynamic.

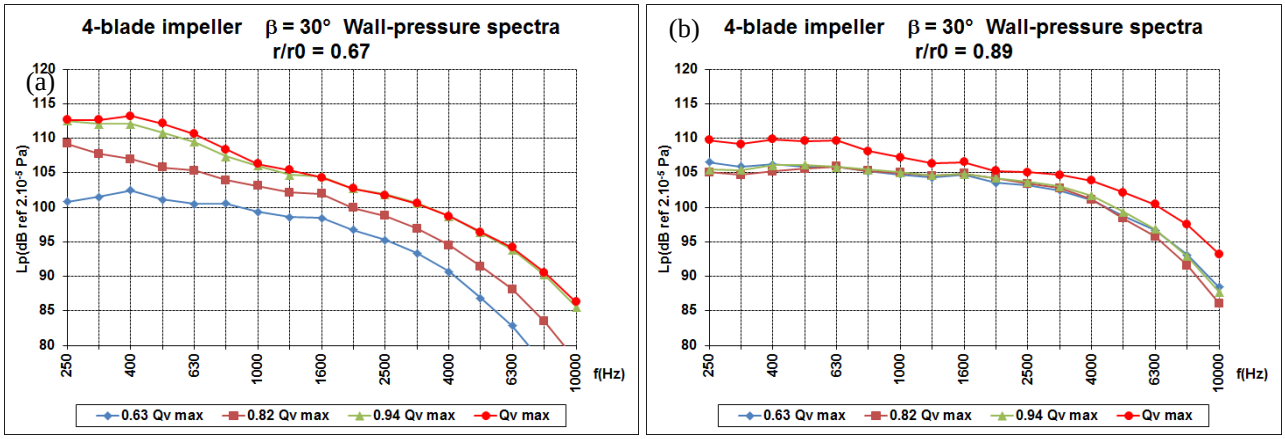

Figure 4 Measured spectra of the wall-pressure fluctuations of the 4-blade fan for β = 30°.
Set of pressure transducers at (a) $r/r_0 = 0.67$, (b) $r/r_0 = 0.89$

Since the prediction input data are experimentally determined at only two radii on the blade span, i.e. 0.67 and 0.89 r_0, an extrapolation is made according to [10] to obtain these data at other radii.

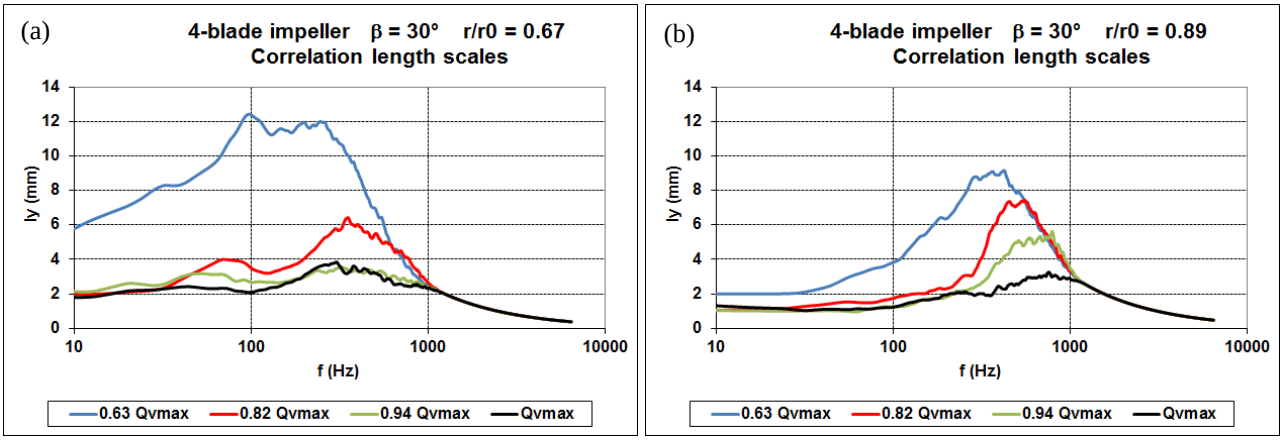

Figure 5 Measured spanwise correlation scales of the wall-pressure fluctuations of the 4-blade fan for β = 30°. Set of pressure transducers at (a) r/r_0 = 0.67, (b) r/r_0 = 0.89

Figure 6 shows the difference between the measured and predicted one-third octave sound power spectra ("inlet + outlet" levels) of the two fans for β = 30° and various operating points. In this figure ΔL_w is always positive whatever the fan and operating point, which means that the prediction always underestimates the sound power spectrum. The difference is quite high at low frequency (f < 200-250 Hz), minimum in the frequency range 250-800 Hz, then re-increases at high frequency.

For the 2-blade impeller (Figure 6-a) the curves ΔL_w are very close to each other, except below 400 Hz at Q_v max. The prediction thus provides a correct trend of the evolution of the sound spectrum with flowrate. That is not the case for the 4-blade fan (Figure 6-b) for which the discrepancies between the curves are much higher. For this fan the gap between the prediction and the experiment is the lowest at Qv max.

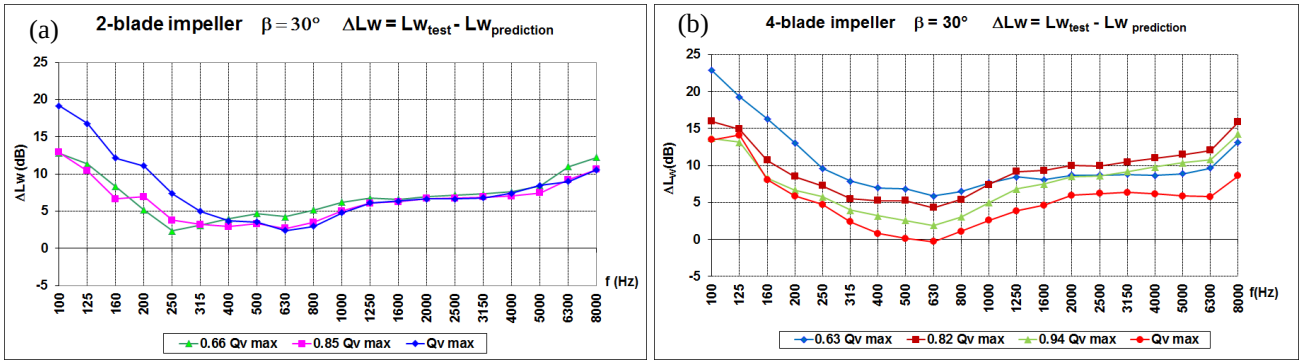

Figure 6 Difference in levels between the measured and predicted sound power spectra for β = 30° and different operating points (a) 2-blade fan, (b) 4-blade fan

Several reasons could explain the systematic underestimation of the prediction compared to the experiment. The first one could be the uncertainty of the input data of the trailing-edge noise model or the non-validity of the model itself. The last reason should be at least partially discarded as the prediction method has been validated by several experiments on stationary airfoils in anechoic wind-tunnels. Furthermore, uncertainties in the input data should lead to overestimations and underestimations of the prediction depending on the blade number, blade angle, operating point and frequency. It is not the case, there is always an underestimation whatever the test configuration.

Another reason could be the contribution of one or several additional noise sources. One may think to an interaction of the inlet turbulence with the blade leading edge due to the motor bracket that

would generate an inflow disturbance. This mechanism is quite unlikely as the bracket is remote from the fan inlet. Nevertheless, an interaction of the turbulence in the boundary layer of the fan casing with the blade tip may not be totally excluded. Tip clearance noise appears as another very good candidate for this additional source. To prove the contribution of this source to the overall fan sound power some further tests have been made.

First, a comparison of the sound power spectra of the 2-blade fan has been made with and without casing (**Erreur ! Source du renvoi introuvable.**). In this case the 2-blade impeller with its shroud and chipboard plate has been disconnected from the wall between the two reverberant rooms and placed in the big inlet room (see Figure 2). The fan operating point for this configuration corresponds to Qv max (zero static pressure). **Erreur ! Source du renvoi introuvable.** shows that the spectrum of the impeller without casing is considerably lower than the spectrum with casing whereas the wall-pressure spectra measured on the blades of both fans are of similar amplitude. The trailing-edge noise prediction without casing tends to overestimate the sound levels unlike the prediction with casing.

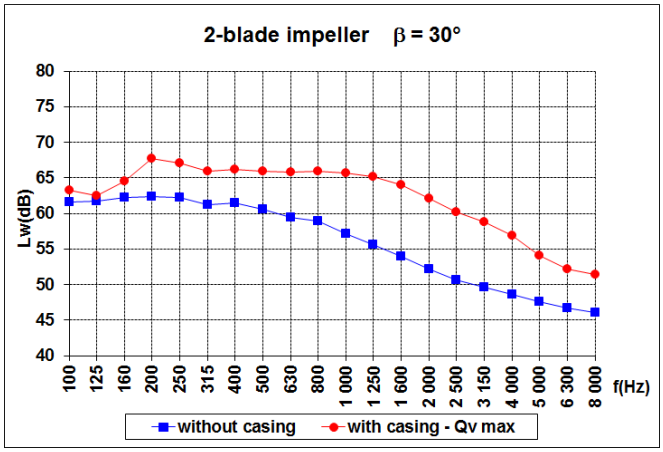

Figure 7 Measured sound power spectra of the 2-blade fan with and without casing in the inlet reverberant room β = 30°

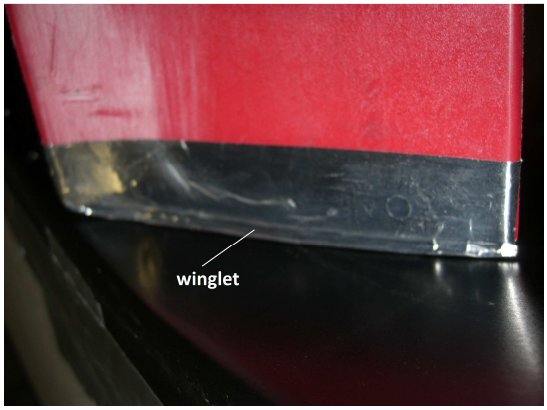

Figure 8 Winglet on the blade pressure side

Other tests have been made on the 2-blade and 4-blade fans to try to reduce the contribution of the tip leakage noise to the overall noise. Based on a research of Bianchi et al. [12] a tip vortex control device (or winglet) has been taped to the pressure side of each blade in the tip region (Figure 8). The aim of this homemade device was to try to counteract the tip leakage flow circulating over the blade tip from the pressure side to the suction side. Figure 9 compares the measured sound power spectra of the 2-blade fan at Qv max with and without winglets. The winglets reduce the sound levels of more than 3 dB in a large frequency range.

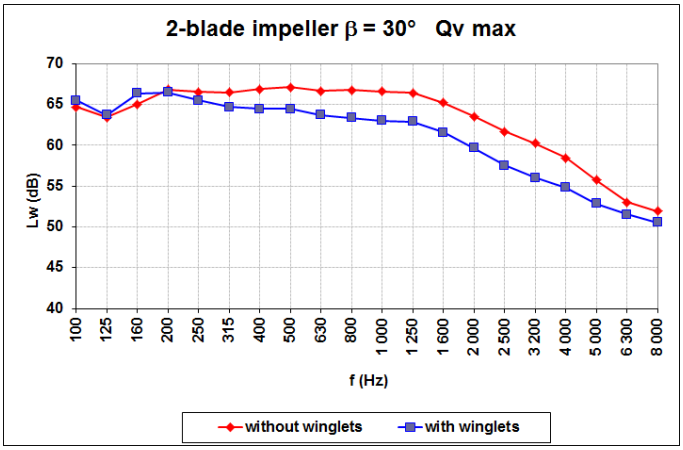

Figure 9 Measured sound power spectra of the 2-blade fan with and without "winglets" β = 30°, Qv max

Figure 10 shows the difference ΔL_w between the measured and predicted sound power levels of the 2-blade and 4-blade fans with and without winglets. With winglets the prediction is much closer to the experiment even if the agreement is still far from perfect. It is not excluded that a tip-clearance noise contribution still exists with the winglets but with reduced amplitude.

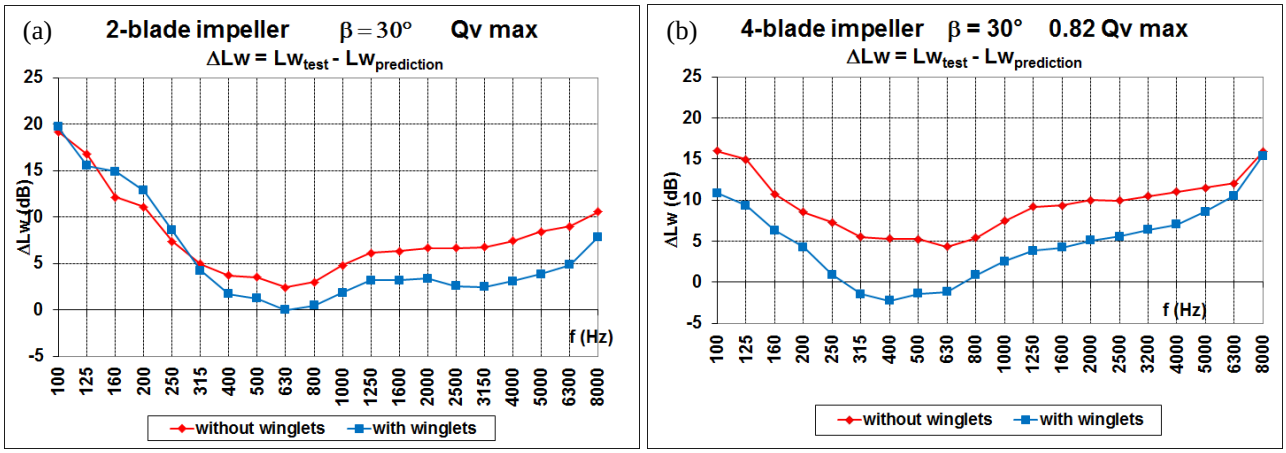

Figure 10 Difference in levels between the measured and predicted sound power spectra with and without winglets β = 30° (a) 2-blade fan at Qv max, (b) 4-blade fan at 0.82Qv max

These results (and others not presented in this paper) prove that the tip-clearance noise strongly contributes to the overall noise radiated by the fans in a way that depends of the blade pitch angle, operating point, and number of blades. To improve the noise prediction of an axial fan it is therefore necessary to develop a model that could be able to predict the tip-leakage noise spectrum. A well-known means to reduce the amplitude of this source on axial fans is to reduce the tip clearance. Unfortunately a reduction of the clearance is often not possible on fans used in industry for design and mechanical reasons. Furthermore, the experience shows that this remedy is sometimes ineffective, especially on propeller fans.

PREDICTION OF THE WALL-PRESSURE SPECTRA

Theoretical background

The trailing-edge noise model used above (equation (1)) requires assessing the spectra of the turbulent wall-pressure fluctuations on the suction side along the blade span close to the trailing edge. As mentioned above these spectra have been measured at two radial locations on the 2-blade and 4-blade fans. The test process is however tricky and expensive, so that it appears worthwhile to try to estimate the spectrum by a model using CFD calculations (RANS simulations) provided that this approach gives reasonably accurate results.

The empirical model used in this study is due to Rozenberg *et al.* [9]. This model, which is an extension of Goody's model [13], takes in account adverse pressure gradient flows such as those on the aft part of the suction side of stationary airfoils or rotating blades. The model has been experimentally validated on isolated airfoils in wind-tunnel [9] but not on rotating blades. The wall-pressure spectrum can be deduced from local parameters of the boundary-layer over the blade at the desired location (i.e. location of the pressure sensors).

According to this model [9] the spectrum of the wall-pressure is given by:

$$\frac{\Phi_{pp}(\omega)U_e}{\tau_{max}^2\delta^*} = \frac{\left[2.82\Delta^2(6.13\Delta^{-0.75}+F_1)^{A1}\right]\left(4.2\frac{\Pi}{\Delta}+1\right)\tilde{\omega}^2}{(4.76\tilde{\omega}^{0.75}+F_1)^{A1}+(C'_3\,\tilde{\omega})^{A2}} \quad (3)$$

where $\tilde{\omega} = \omega\delta^*/U_e$, $\omega = 2\pi f$, δ^* is the boundary-layer displacement thickness, U_e the flow velocity outside the boundary-layer and τ_{max} the maximum shear stress.

The other terms in equation (3) depend on the following parameters, in addition to those mentioned above: boundary-layer thickness (δ), boundary-layer momentum thickness (θ), friction velocity (u_τ) and mean wall-pressure gradient in the streamwise direction (dp/dx).

The objective of this part of the study is therefore to compare the predicted and measured wall-pressure spectra written under the following non-dimensional form:

$$\tilde{\Phi}_{pp}(\tilde{\omega}) = \frac{\Phi_{pp}(f)}{\pi U_e^3 \delta^* \rho_0^2} \quad (4)$$

with ρ_0: air density. The non-dimensional spectrum is thus $\tilde{\Phi}_{pp}(\tilde{\omega}) = \Phi_1(\omega) - 10\lg\left(\frac{\rho_0^2 U_e^4}{2\tau_{max}^2}\right)$

where $\Phi_1(\omega)$ is the right-side member of equation (3).

CFD simulations

Model and boundary conditions

A stationary three-dimensional CFD RANS modeling of the 4-blade axial fan is conducted in order to obtain the parameters of the boundary layer. Due to the complexity of the geometry, a hybrid mesh approach is adopted. The mesh features a refined mesh close to the fan, with prismatic layers in the blade-wall region (Figure 11 (b)), and a coarser unstructured tetrahedral mesh towards the end of the calculation domain (Figure 11 (a)). The final volume mesh grid of the calculation domain consists of 21.2 M elements. The Navier–Stokes equations with k-ω SST turbulence model are used for calculation. The simulations were done with commercial code Fluent 14.

(a)

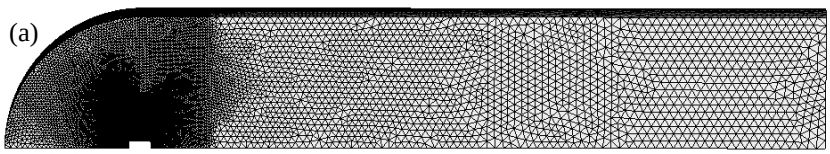

(b)

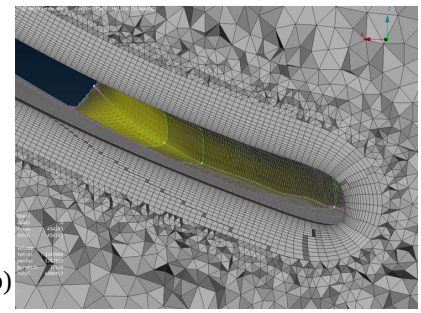

Figure 11: Calculation domain mesh (a) volume mesh

(b) zoom of the mesh in the blade area,

The computation domain and the boundary conditions used are illustrated in Figure 12. The fan, in its actual test facility, is modeled with the multiple reference frame approach (MRF). The fluid region in the fan area is modeled in a rotating reference frame and the fluid surrounding the fan area is modeled in a stationary frame [14]. The limit of the MRF region is shown in Figure 12. The Inlet boundary condition is “Stagnation Inlet” with total pressure equal to zero and the Outlet boundary is “Mass Flow Outlet” imposed. The fan walls are modeled as rotating walls with zero velocity relative to the adjacent cell zone. The other walls of the domain are modeled as stationary walls. The fluid in the MRF region is rotating at the fan speed, i.e. 600 rpm. To reduce the problem size

the flow field is simulated for a single blade passage by using periodic boundary conditions; the calculation domain corresponds to a quarter of the total domain. Simulations are performed for 4 fan operating points.

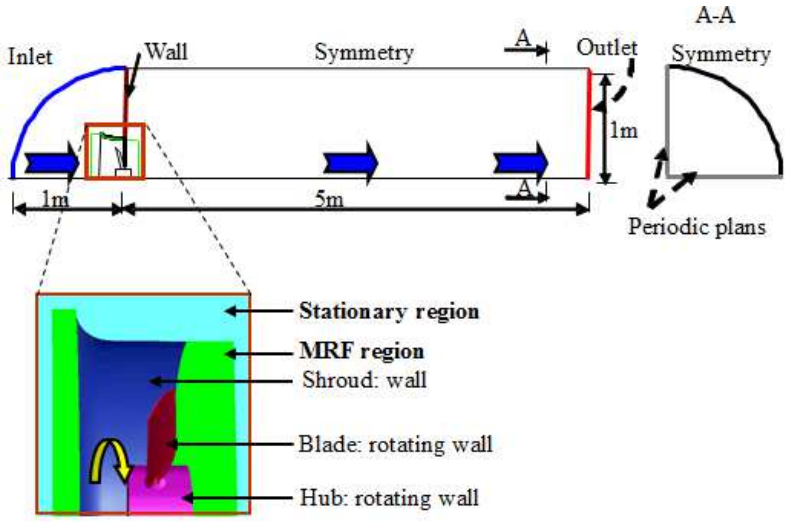

Figure 12 Dimensions and boundary conditions of the calculation domain

Results

Figure 13 shows examples of results obtained with the RANS simulations. Cartography of the relative velocity magnitude in section r/r0 = 0.67 is presented in Figure 13 (a). The boundary layer development is clearly visible. The leading edge separation bubble on the suction side is captured by numerical simulation. The black straight line reproduces the normal to the blade surface along which velocity profiles are extracted to allow the calculation of the boundary layer characteristics.

Figure 13 (b) shows the tip vortex which detaches from the blade in the forward part of the chord. Another potential noise source due to the interaction of this vortex with the adjacent blade may not be excluded. In the latter case the winglets mentioned in the first part of the paper might have some effect on this interaction and the resulting potential noise.

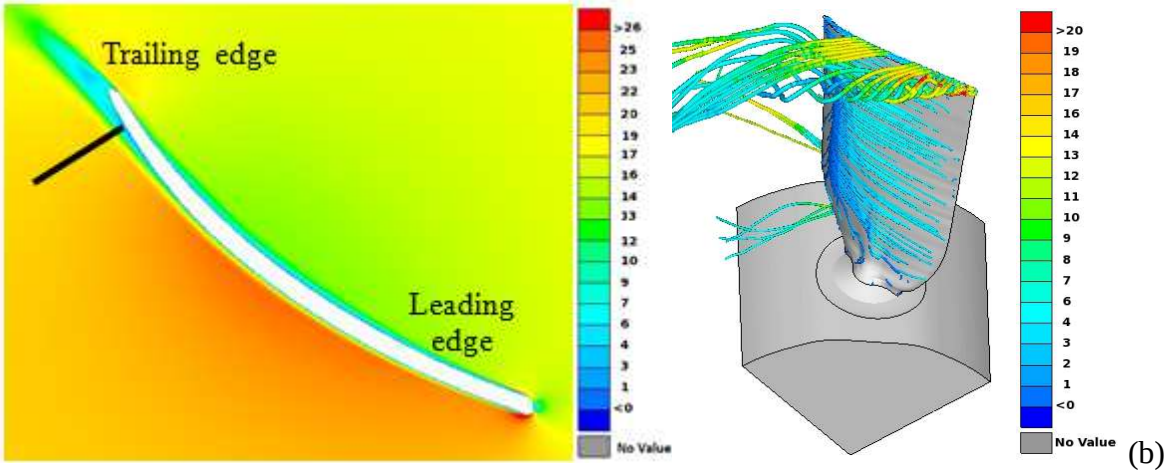

(a) (b)

Figure 13: Examples of RANS simulation results for Qv= 0.82 Qv max and β = 30°
(a) Relative velocity magnitude in the mid-span section; (b) Path lines on the blade tip

Table 2 gives the boundary layers parameters extracted from CFD simulations. These data are used to deduce the wall-pressure spectra on the blade.

Table 2 Boundary layer parameters deduced from CFD simulations for the 4-blade fan at β = 30°

	Qv max		0.94 Qv max		0.82 Qv max		0.63 Qv max	
r/r0	**0.67**	**0.89**	**0.67**	**0.89**	**0.67**	**0.89**	**0.67**	**0.89**
U_e (m/s)	21.1	26.5	21.0	26.0	20.3	24.0	18.0	23.2
δ (mm)	5.00	4.72	4.57	4.88	5.45	5.83	13.72	12.92
δ* (mm)	2.02	1.62	1.93	1.66	2.18	1.97	5.55	3.33
θ (mm)	0.70	0.63	0.70	0.67	0.76	0.76	2.39	0.65
Δ = δ/δ*	2.5	2.9	2.4	2.9	2.5	3.0	2.5	3.9
H = δ*/θ	2.9	2.9	2.7	2.9	2.9	2.9	2.3	2.8
τ_{max} (Pa)	0.512	0.377	0.451	0.286	0.451	0.213	0.859	0.504
τ_w (Pa)	0.578	0.488	0.520	0.384	0.514	0.296	0.896	0.521
u_τ (m/s)	0.69	0.64	0.66	0.57	0.65	0.50	0.86	0.66
dp/dx	2620	7373	2667	4717	2353	3278	812	1572

Experimental validation of the wall-pressure spectra

Examples of predicted and measured spectra of wall-pressure fluctuations are shown in Figure 14 for the 4-blade impeller at β = 20°, 0.8 Qv max and the two spanwise locations r/r0 = 0.67 and 0.89. Figure 15 shows a similar comparison for β = 30° and 0.82 Qv max. The prediction underestimates the amplitude of the spectrum whatever the frequency and the case considered. The difference in level between the two spectra, which varies from 0 dB to more than 20 dB, depends of the blade angle, flowrate, radial location and frequency.

These discrepancies may be due to uncertainties on:

- the measured pressure fluctuations
- the assessment of the boundary layer characteristics deduced from the RANS simulations
- the validity of the empirical model of Rozenberg *et al*.

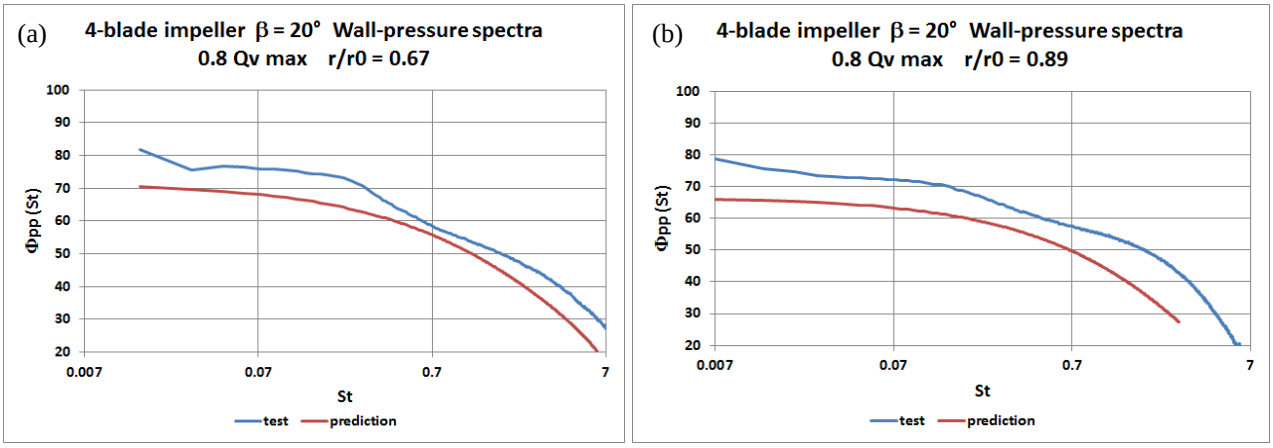

Figure 14 Comparison of the measured and predicted wall-pressure spectra of the 4-blade fan, β = 20°, 0.8 Q_v max (a) r/r_0 = 0.67 (b) r/r_0 = 0.89

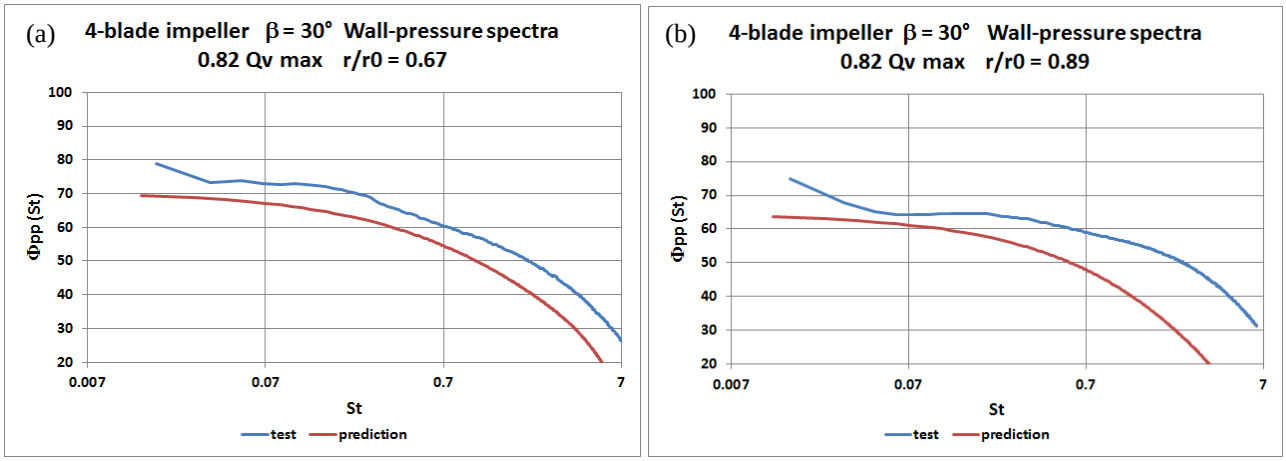

Figure 15 Comparison of the measured and predicted wall-pressure spectra of the 4-blade fan, β = 30°, 0.82 Q_v max (a) r/r_0 = 0.67 (b) r/r_0 = 0.89

Two boundary layer parameters have a large impact on the amplitude and shape of the wall-pressure spectra, namely the maximum shear stress τ_{max} and the pressure gradient dp/dx. An increase of the amplitude of these parameters as compared to those obtained by CFD simulations allows reducing the gap between the prediction and the experiment in a significant way.

More work is needed to understand the actual reasons of this disagreement. The von Karman Institute, which is with Cetim a partner of CETIAT in this research programme, is currently making CFD simulations and estimation of the wall-pressure spectra on the 4-blade fan by another model than the Rozenberg's model. A comparison of their predictions with those of the present paper could be helpful to improve the modeling.

CONCLUSIONS

The prediction of the broadband noise of axial fans requires diagnosing the main noise sources of the fan, developing models of these sources and getting the appropriate input data of the models. In the present study the diagnosis of the sources is partially achieved: the main noise mechanisms are likely trailing-edge noise and tip clearance noise but it is not excluded that other sources may provide a contribution to the overall sound power spectrum of the fan, depending on the operating point, blade pitch angle, blade number, and frequency. The interaction of the inlet turbulence of the casing with the blade leading edge might be a potential additional source as well as the interaction of the tip vortex with the adjacent blade.

An analytical model of trailing-edge noise based on an extension of Amiet's formulation, which was experimentally validated on steady airfoils in wind tunnels, has been applied on the test fans. A comparison of results predicted from this model and experimental results shows a systematic underestimation of the prediction, which confirms that other sources may contribute to the fan noise. A perturbation of the tip leakage flow by homemade devices allows reducing the amplitude of this underestimation in a large frequency range, which proves that tip clearance noise is also a major contributor. Unfortunately no analytical model is currently available to predict this mechanism that is not yet fully understood.

The spectra of the pressure fluctuations on the suction side of the blades near the trailing edge are the main input data of the trailing-edge noise model used in this study. The experimental validation of an empirical model due to Rozenberg et al. to predict these spectra with input data deduced from steady CFD simulations is currently not satisfactory on the present fans. Further work is needed to understand the discrepancies between the predicted and measured spectra on the blades.

BIBLIOGRAPHY

[1] M. Roger – *Broadband noise from lifting surfaces – Analytical modeling and experimental validation.* CISM International Centre for Mechanical Sciences, Vol. 545, pp. 289-344, **2013**

[2] M. Roger, S. Moreau – *Back-scattering correction and further extensions of Amiet's trailing-edge noise model. Part 1: Theory*. J. Sound Vib., 286(3), pp. 477-506, **2005**

[3] M. Roger, S. Moreau, A. Guédel – *Broadband fan noise prediction using single-airfoil theory.* Noise Control Eng. J., 54(1), pp. 5-14, **2006**

[4] M. Roger, S. Moreau – *Extension and limitations of analytical airfoil broadband noise models.* Aeroacoustics, 9(3), pp. 273-305, **2010**

[5] R.H. Schlinker, R.K. Amiet – *Helicopter rotor trailing edge,* NASA Tech. Rep. CR – 3470, **1981**

[6] A. Guédel, Y. Rozenberg, M. Roger, G. Perrin – *Experimental validation of a model of fan trailing-edge noise,* Noise Control Eng. J., 57(4), pp. 318-326, **2009**

[7] Y. Rozenberg, S. Moreau, M. Henner, S.C. Morris – *Fan trailing-edge noise prediction using RANS simulations,* AIAA Paper 2010-3720, **2010**

[8] T. Carolus, M. Schneider, H. Reese **–** *Axial flow fan broad-band noise and prediction,* J. Sound Vib., 300, pp. 50-70, **2007**

[9] Y. Rozenberg, G. Robert, S. Moreau – *Wall-pressure spectral model including the adverse pressure gradient effects*, AIAA J. 50(10), pp. 2168-2179, **2012**

[10] Y. Rozenberg, M. Roger, S. Moreau – *Rotating blade trailing-edge noise: experimental validation of analytical model*, AIAA J. 48(5), pp. 951-962, **2010**

[11] S. Sinayoko, M. Kingan, A. Agarwal – *Trailing edge noise theory for rotating blades in uniform flow*, Proc. Roy. Soc. A 469: 20130065, **2013**

[12] S. Bianchi, A. Corsini, F. Rispoli, A.G. Sheard - *Near-field aeroacoustic investigations of axial fan with tip end plates,* Proc. Internoise 2008, Shangai, **2008**

[13] M. Goody – *Empirical spectral model of surface pressure fluctuations,* AIAA J. 42(9), pp. 1788-1794, **2004**

[14] A. Guédel, M. Robitu, N. Descharmes, D. Amor, J. Guillard – *Prediction of the blade trailing-edge noise of an axial flow fan,* Proc. ASME Turbo Expo 2011, Vancouver, GT2011-45256, **2011**